Journal of Materials Chemistry B

Accepted Manuscript

ROYAL SOCIETY OF CHEMISTRY

www.rsc.org/materialsB

Synthesis and characterization of novel TiO_2-poly(propylene fumarate) nanocomposites for bone cementation

Mehrnaz Salarian[1], William Z. Xu[2], Mark C. Biesinger[3], and Paul A. Charpentier[1, 2, *]

[1] Biomedical Engineering Graduate Program, University of Western Ontario, London, Ontario, Canada, N6A 5B9

[2] Chemical and Biochemical Engineering Department, University of Western Ontario, London, Ontario, Canada, N6A 5B9

[3] Surface Science Western, University of Western Ontario, 999 Collip Circle, LL31, London, Ontario, Canada, N6G 0J3

Abstract

This work reports on a new methodology for synthesizing poly(propylene fumarate) (PPF)/titania nanowire composites which would be beneficial in tissue engineering for orthopaedic bone cements. The synthetic procedure reacted PPF with maleic anhydride to create HOOC-PPF-COOH species in a ring-opening reaction at room temperature. These species were then coordinated to titania nanowires by metal carboxylate bonding through the end -COOH groups. These PPF-grafted nano-TiO_2 assemblies were then further polymerized and crosslinked in the presence of N-vinylpyrrolidone to produce the bone cements. The synthesis and modification of PPF was confirmed by NMR (^{1}H and ^{13}C) and XPS, while the reaction chemistry of the functionalized PPF and nano-TiO_2 was also investigated by XPS and FTIR. Mechanical testing of the resulting composites demonstrated a significant reinforcement of the tensile and flexural properties, showing the utility of this synthetic approach for bone tissue engineering.

Keywords: TiO_2 nanofibers, Poly(propylene fumarate), Functionalization, Maleic anhydride, Nanocomposite, Mechanical enhancement, Bone cement

1. Introduction

Developing new materials for bone cementation and bone tissue engineering is of emerging scientific interest,[1] requiring new synthetic approaches that provide both mechanical strength and biocompatibility.[2] Driving forces include our longer life spans and the potential to treat skeletal bone defects and diseases such as osteonecrosis, which is caused by the temporary or permanent loss of blood supply to bone.[3] Cementation involves the injection of a liquid polymeric material, which hardens in the defect, providing mechanical support to the bone.[4] The most universally used injectable bone cement is made of poly(methyl methacrylate) (PMMA).[5-7] However, there are several drawbacks associated with PMMA bone cements including: (1) exothermic polymerization that can lead to impaired local blood circulation and thermal necrosis of the surrounding bone, (2) release of unreacted MMA monomer leading to chemical necrosis of the bone, (3) non-biodegradability, so PMMA cannot be replaced with new bone formation, and (4) non-bioinertness.[8] Recently, poly(propylene fumarate) (PPF) has attracted considerable interest as a promising biodegradable material for treating skeletal defects.[9-11] PPF is a linear and unsaturated polyester containing one unsaturated C=C double bond per repeating unit. The double bonds of PPF can crosslink with itself or a variety of crosslinking agents such as 1-vinyl-2-pyrrolidinone (N-VP) to form crosslinked polymer networks.[12, 13] In addition, the ester linkage allows for hydrolysis of the polymer into biocompatible and excretable degradation products of fumaric acid and propylene glycol, shown in scheme 1.[14, 15]

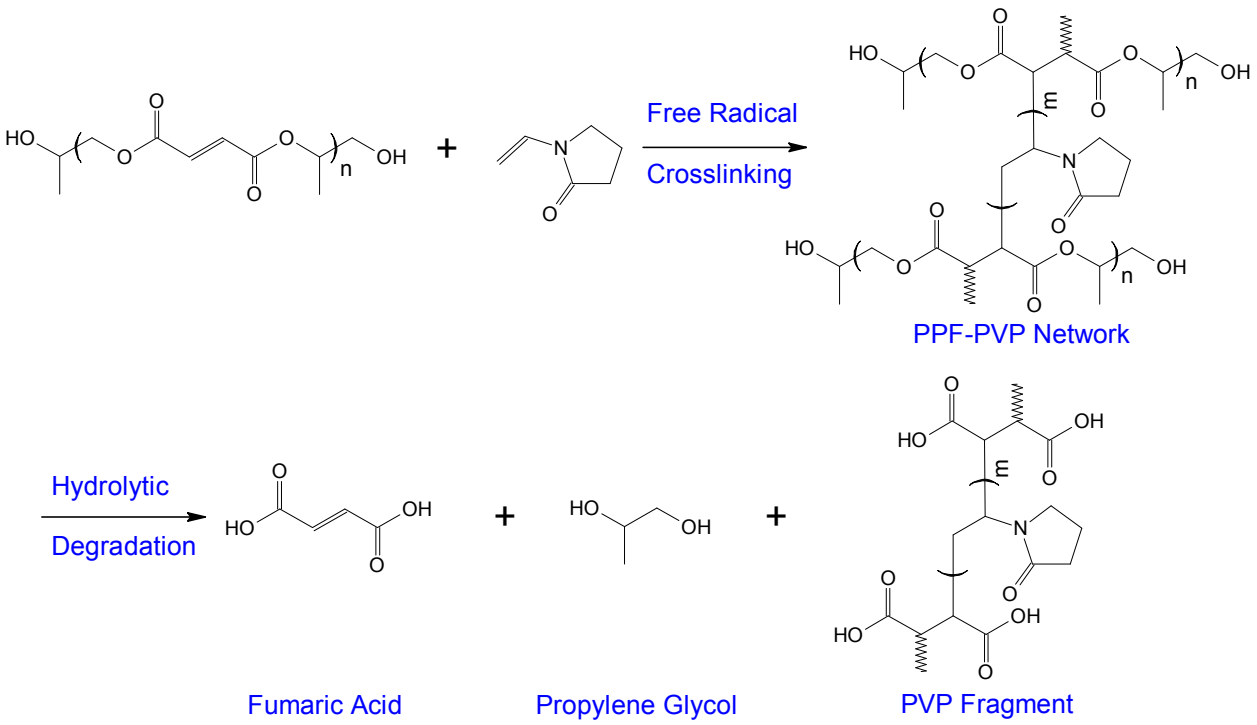

Scheme 1. Crosslinking and degradation scheme of PPF-PPF-PVP networks.

Even though crosslinked PPF can be considered as a material for trabecular bone tissue regeneration, significant mechanical reinforcement is needed for the use of this material under load bearing conditions.[16, 17] Nanoparticles such as calcium phosphates including tetracalcium phosphate (TTCP), dicalcium phosphate (DCPA), and hydroxyapatite (HAp) have been investigated for PPF-based cements, enhancing the mechanical strength of the composite and osteoconductivity.[18-20] Shi et al. and Sitharaman et al. used single-walled carbon nanotubes (SWNTs) as reinforcing fillers in PPF because of their excellent mechanical properties and high aspect ratios; however, the addition of carbon nanotubes may impose negative effects on the aesthetic requirements and biocompatibility of the bone cement.[16, 21] It is believed that one-dimensional oxides, such as nanowires or nanotubes of SiO_2, ZrO_2, Al_2O_3, and TiO_2 would be promising for the reinforcement of bone cement compositions due to their unique properties and low cost compared to carbon nanotubes.[22, 23] Horch et al. and Mistry et al. designed a composite

material utilizing surface-modified carboxylate alumoxane nanoparticles and PPF network, which showed a significant improvement in flexural properties.[17, 24] However, alumina-based implants have rarely shown to initiate apatite formation and cannot directly attach to bone.[25, 26] Essentially no studies have examined the incorporation of 1D nano-structured oxides into PPF bone cement matrix to enhance its mechanical properties. To the best of our knowledge, this is the first study to incorporate 1D nano-structured titania, into a PPF matrix, which requires a new synthetic methodology. TiO_2 nanofibers or wires are expected to be superior to alumina nanoparticles owing to their excellent biocompatibility and unique oseointegration. Titania nanofibers or wires can directly bond to bone through the formation of a biologically active bone-like apatite layer on the surfaces of implants within the body (oseointegration).[26, 27] In addition, titania nanofibers or wires have high aspect ratios which enhances their interfacial interaction with the resin matrix leading to dramatically enhanced mechanical properties.[23, 28]

In this work we present a new method for the synthesis of functionalized PPF containing a carboxyl group at each end of the PPF chains using a ring opening reaction at room temperature in the presence of a highly nucleophilic tertiary amine catalyst, 4-dimethylaminopyridine.[29, 30] The carboxyl group allowed for coordination of PPF to nano-TiO_2, and the subsequent crosslinking reaction with 1-vinyl-2-pyrrolidinone to form crosslinked TiO_2-PPF nanocomposites. The mechanical properties of the synthesized crosslinked TiO_2-PPF nanocomposites were measured, showing potential applications in bone cementation.

2. Experimental details

2.1. Materials

Titanium isopropoxide (99.999%), glacial acetic acid (>99.7%), diethyl fumarate (98%), propylene glycol (1,2-propanediol) (≥99.5%), anhydrous zinc chloride ($ZnCl_2$, ≥99.995%), hydroquinone (99%), maleic anhydride (95%), 4-dimethylaminopyridine (DMAP), hydrochloric acid (37%), anhydrous magnesium sulfate (99.0%), anhydrous diethyl ether (≥99.0%), anhydrous dichloromethane (DCM, ≥99.8%), anhydrous tetrahydrofuran (THF, ≥99.9%), 1-vinyl-2-pyrrolidinone (N-VP), benzoyl peroxide (BPO), and N-dimethyl-p-toluidine (DMT) were purchased from Sigma-Aldrich Canada and used as received. Instrument grade carbon dioxide (99.99%) was purchased from BOC Canada.

2.2. Characterization

Surface characterization: Scanning electron microscopy (SEM) images were collected using a Leo(Zeiss) 1540XB SEM. Imaging was performed at either low voltage (1 kV) for morphology or at 10 kV for backscatter imaging. Samples were coated with 5nm of osmium metal in a Filgen OPC80T. For studying the fracture surface, samples were broken by submersing in liquid nitrogen in a stainless steel mortar and broken with a stainless steel pestle. The particle diameter and aspect ratio frequency distribution of TiO_2 nanoparticles were obtained by measuring over 100 TiO_2 nanoparticles using Image J software (NIH, version 1.37). Transmission electron microscopy (TEM) images were recorded using a Philips CM10 transmission electron microscope with an AMT digital camera (Eindhoven, Netherlands) operated at 100 kV. **Spectroscopic examinations:** Attenuated total reflection-Fourier transform infrared (ATR-

FTIR) spectra were measured using a Nicolet 6700 FTIR spectrometer (Thermo Scientific) equipped with a smart iTR (diamond ATR). The spectra were recorded in the range of 600-4000 cm^{-1} with a resolution of 4 cm^{-1} over 32 scans. X-ray photoelectron spectroscopy (XPS) analyses were carried out with a Kratos AXIS Ultra spectrometer using a monochromatic Al K(α) source (15mA, 14kV). Samples were placed on a carbon-based double-sided adhesive tape for analysis. The Kratos charge neutralizer system was used on all specimens. Survey scan analyses were carried out with an analysis area of 300 μm × 700 μm and a pass energy of 160 eV. High resolution analyses were carried out with an analysis area of 300 μm × 700 μm and a pass energy of 20 eV. Spectra were charge corrected to the main line of the carbon 1s spectrum set to 284.8 eV. Spectra were analyzed using CasaXPS software (version 2.3.14). ^{1}H and ^{13}C NMR spectra were measured using either a Varian INOVA 600 or a Varian INOVA 400 spectrometer at 25 ^{o}C. $CDCl_3$ was used as the solvent and chemical shifts were referenced to tetramethylsilane (TMS; 0.0 ppm).

Thermal characterization: Thermogravimetric analysis (TGA) was performed using a TA Q500 TGA at a heating rate of 10 ºC/min under an inert (nitrogen) atmosphere.

Determination of mechanical properties: Mechanical tensile properties were measured using an Instron 5943 universal testing machine (Instron, Canton, MA) equipped with a 500 N (tension) load cell. Tensile testing was conducted in accordance with ASTM D638-91a. Dogbone specimens with overall length of 60 mm and width of grip section of 10 mm were used for tensile testing. Stress-strain relationship was obtained from the load and displacement data. Young's modulus was determined by calculating the slope of the linear portion of the stress-strain curve, and tensile strength was defined as the maximum applied stress prior to failure. For each group, 5 independent specimens (n=5) were tested in tension at a crosshead speed of 10

mm/min. Flexural strength (FS) and flexural modulus (FM) of the nanocomposites were determined in accordance with ASTM D790M-92 using a dynamic mechanical analyzer, DMA Q800 (TA instruments). Flexural testing samples, rectangular bar specimens (n=5) (50 mm × 25 mm × 2 mm), were placed on a three-point bending apparatus with two supports spanning 40 mm from each other and loaded at the cross-head speed of 10 mm/min to the center of each specimen until failure. In an approach similar to that of tensile testing, flexural modulus was calculated as the slope of the initial linear region of the stress-strain curve, while flexural fracture strength was determined as the maximum applied stress prior to failure.

2.3. Preparation of materials

2.3.1. Synthesis of poly(propylene fumarate) (PPF)

PPF was synthesized using a two-step transesterification method described in the literature.[31] In a typical experiment, diethyl fumarate (31.56 g, 183 mmol) and propylene glycol (41.38 g, 549 mmol) were reacted in an inert atmosphere under stirring, with $ZnCl_2$ (0.250 g, 1.83 mmol) and hydroquinone (0.0403 g, 0.366 mmol) being added as a catalyst and a crosslinking inhibitor, respectively. After the reaction temperature had been increased to 110 ºC, the temperature was further increased from 110 ºC to 150 ºC in an increment of 10 ºC every 15 min. Bis(hydroxypropyl) fumarate (**1**) was formed with the continuous removal of the byproduct ethanol, as a distillate. This step was terminated by cooling down to 100 ^{o}C when ~ 90% of the theoretical yield of ethanol was collected.

The second step of the reaction, transesterification of the intermediate bis(hydroxypropyl) fumarate to form PPF (**2**), was conducted under reduced pressure (<1 mm Hg), producing

propylene glycol as a byproduct. The temperature was raised gradually from 100 ºC to 150 ºC in an increment of 10 ºC every 30 min, and the reaction proceeded until the desired molecular weight of PPF was obtained. The polymer product was then dissolved in dichloromethane followed by several acid washes with a 5% v/v solution of 1 N HCl, two washes with distilled water, and two washes with brine. After drying with magnesium sulfate, the organic phase was concentrated by rotary evaporation and then precipitated in diethyl ether to remove the hydroquinone inhibitor. The precipitated polymer was washed with diethyl ether and dried under vacuum. Yield: 73% (21 g). FTIR (cm^{-1}): 1713 ($\nu_{C=O}$), 1645 ($\nu_{C=C}$), 1251 ($\nu_{C-O-C(as)}$), 1148 ($\nu_{C-O-C(s)}$). ^{1}H NMR ($CDCl_3$, 600 MHz) δ (ppm): 6.85 (O=C-C<u>H</u>=C<u>H</u>-C=O), 5.29 (O-C<u>H</u>(CH_3)-CH_2), 4.33 & 4.25 (O-CH(CH_3)-C<u>H</u>$_2$), 1.34 (O-CH(C<u>H</u>$_3$)-CH_2), 5.10, 4.22, 4.09, 3.70, 1.29, and 1.23 (end groups of the PPF polymer chain). ^{13}C NMR (CDCl3, 100 MHz) δ (ppm): 164.0-164.3(O=<u>C</u>-CH=CH-<u>C</u>=O), 133.3-134.0 (O=C-<u>C</u>H=<u>C</u>H-C=O), 69.2 (O-<u>C</u>H(CH_3)-CH_2), 66.6 (O-CH(CH_3)-<u>C</u>H$_2$), 16.3 (O-CH(<u>C</u>H$_3$)-CH_2), 73.1, 70.3, 65.8, 65.5, 19.2, and 16.0 (end groups of the PPF polymer chain).

2.3.2. Functionalization of PPF

In order to functionalize the PPF chain with maleic anhydride, to a solution of PPF (1g, 0.91 mmol of -OH group) in 10 mL of anhydrous dichloromethane were added DMAP (0.11 g, 0.91 mmol) and maleic anhydride (0.36 g, 3.64 mmol). The reaction mixture was stirred under argon at room temperature for 24 h. After completion of the reaction, 5 mL of dichloromethane was added to the flask followed by washing with 10 mL of 1 N HCl solution and distilled water. The organic phase was subsequently dried over anhydrous magnesium sulfate. After that, the organic phase was filtered and the solvent was removed by rotary evaporation to afford maleic anhydride-functionalized PPF (MA-PPF) (**3**). Yield: 59% (0.64g). ^{1}H NMR ($CDCl_3$, 600 MHz) δ

(ppm): 8.19 (-COOH). 6.85 (O=C-CH=CH-C=O), 5.29 (O-CH(CH_3)-CH_2), 4.33 & 4.25 (O-CH(CH_3)-CH_2), 1.34 (O-CH(CH_3)-CH_2). ^{13}C NMR ($CDCl_3$, 100 MHz) δ (ppm): 164.0-164.3(O=C-CH=CH-C=O), 133.3-134.0 (O=C-CH=CH-C=O), 69.2 (O-CH(CH_3)-CH_2), 66.6 (O-CH(CH_3)-CH_2), 16.3 (O-CH(CH_3)-CH_2).

2.3.3. Synthesis of TiO_2 nanofibers via sol-gel reaction in supercritical CO_2

High surface area TiO_2 nanofibers were synthesized using supercritical CO_2 ($scCO_2$) as reported by Sui et al.[32] Briefly, in a typical experiment, titanium isopropoxide (1 g) was quickly placed in a 10-mL stainless steel view cell, followed by addition of acetic acid (4 g). CO_2 was then added to the view cell using a syringe pump (Isco 260D) to the desired pressure (6000 psig) while increasing the temperature to 60 °C. A magnetic stirrer was used for mixing the reaction mixture. Stirring was stopped after 24 h, and normally several days of aging were required for a complete reaction. After aging, the formed gel was washed continuously using 80 mL of CO_2 at a rate of approximately 0.5 mL/min, followed by controlled venting at 0.5 mL/min to prevent collapse of the solid network. The as-prepared powder was calcined at 450 °C in air for 2 h with a heating rate of 10 °C/min and a cooling rate of 0.5 °C/min to room temperature. The calcined powder was kept in a vacuum oven at 80 °C.

2.3.4. Synthesis of TiO_2-PPF nanocomposites

To prepare TiO_2-PPF nanocomposites (**4**), 0.5, 1.25, or 2.5 wt% of the synthesized TiO_2 nanofibers (0.005, 0.0125, or 0.0250 g) was dispersed in 20 mL of THF with the aid of ultrasonic agitation for 1 h, followed by reacting with the above synthesized MA-PPF (1 g) at 70 °C under argon with constant stirring for 24 h. After filtering off the solvent and the unreacted MA-PPF, the product was further purified by dispersion in THF, centrifugation, and removal of the

supernatant. This purification process was repeated several times until the supernatant became clear. Finally, the resulting solid product was dried at 55 ºC under vacuum overnight. The composition of the synthesized nanocomposites and the nano-TiO_2 concentration in each nanocomposite formulation reviewed by TGA analysis are presented in Table 1.

FTIR (cm^{-1}): 1713 ($\nu_{C=O}$), 1645 ($\nu_{C=C}$), 1570 & 1377 ($\nu CO_2^-{}_{(as)}$), 1251 ($\nu_{C-O-C(as)}$), 1165 ($\nu\ CO_2^-{}_{(s)}$), 1148 ($\nu_{C-O-C(s)}$).

Table 1: Formulation of the TiO_2-PPF nanocomposites.

MA-PPF (g)	**nano-TiO_2 (g)**	***nano-TiO_2 wt% in the synthesized nanocomposite**	**Sample Name**
1 g	0.005 g	5 wt%	TiO_2-PPF nanocomposite-1
1 g	0.0125 g	10 wt%	TiO_2-PPF nanocomposite-2
1 g	0.0250 g	22 wt%	TiO_2-PPF nanocomposite-3

Note: * the weight percentage of nano-TiO_2 in each TiO_2-PPF nanocomposite formulation is obtained from the TGA analysis.

For comparison of XPS study, a mechanically mixed PPF-TiO_2 nanocomposite was fabricated by mechanical mixing of the PPF (1 g) and TiO_2 nanoparticles (0.10 g).

2.3.5. Synthesis of bone cement composites

The bone cement composites (**5**) were prepared by crosslinking the synthesized TiO_2-PPF nanocomposites (details are provided in Table 1) using N-VP. In a typical experiment, the above

synthesized TiO_2-PPF nanocomposite (1 g) was mixed with N-VP (0.4 g) for 2 h. Initiator, BPO (0.05 g), was dissolved in 250 µL of N-VP. The 50 µL of BPO solution was then combined and mixed with the TiO_2-PPF nanocomposite solution. Subsequently, 40 µL of accelerator solution (20 µL of DMT in 980 µL of dichloromethane) was added with rapid mixing to accelerate the crosslinking reaction.[4, 19] The resulting paste was placed in a Teflon mold, then loaded in an oven at 60 °C for 1 h to facilitate crosslinking. After that, the mold was cooled down to room temperature, and the formed bone cement composite was removed before being subject to mechanical testing. Three different bone cement composites were prepared using the TiO_2-PPF nanocomposites synthesized with different amounts of TiO_2, which are listed in Table 2.

For comparison of mechanical testing, bone cement composites were prepared by crosslinking the mechanically mixed 1 g of PPF and 0.05 g of nano-TiO_2 (corresponding to the actual TiO_2 concentration in the TiO_2-PPF nanocomposite-1 reviewed by TGA analysis represented in Table 1) following the above procedure. The composition of the prepared mechanically mixed bone cement composite is also listed in Table 2.

Table 2: Formulation of the bone cement composites.

Entry No.	TiO_2-PPF	nano-TiO_2	PPF	Formed Product
1			1 g	Crosslinked PPF
2	1 g of TiO_2-PPF synthesized using 0.005 g of TiO_2			Bone cement composite-1
3	1 g of TiO_2-PPF synthesized using 0.0125 g of TiO_2			Bone cement composite-2
4	1 g of TiO_2-PPF synthesized using 0.0250 g of TiO_2			Bone cement composite-3

5		0.05 g	1 g	Mechanically mixed bone cement

Note: Additionally, 0.4 g of N-VP, 50 μL of BPO solution, and 40 μL of DMT solution were added in the preparation of these materials.

3. Results and Discussion

3.1. Synthesis and functionalization of PPF

The synthesis of PPF involves firstly a transesterification reaction of diethyl fumarate with propylene glycol (Step **a** in Scheme 2) to produce bis(hydroxypropyl) fumarate (**1**). In step **b**, poly(propylene fumarate) (PPF) (**2**) is produced by the transesterification/polymerization of **1** with $ZnCl_2$/hydroquinone. In this step, the alkoxy group of the intermediate, bis(hydroxypropyl) fumarate), is replaced with an alcohol from a second bis(hydroxypropyl) fumarate intermediate, propagating PPF polymerization and producing propylene glycol as a byproduct. The synthesized PPF was then reacted with maleic anhydride to form maleic anhydride-functionalized PPF (MA-PPF) (**3** of Scheme 2). A small amount of $ZnCl_2$ was added in the transesterification reaction as a catalyst, while a small amount of hydroquinone was added as an inhibitor to prevent the C=C double bond from being polymerized at high temperatures up to 150 °C. Continuous removal of the byproducts ethanol in the first transesterification reaction and propylene glycol in the second transesterification reaction as the condensates is necessary to drive the step-growth condensation polymerization reactions. The esterification reaction of maleic anhydride and PPF provided PPF with a functional carboxyl group at both ends of the polymer chains **(3**), in order to provide potential coordination of the functionalized PPF to the surface of TiO_2 nanofibers.

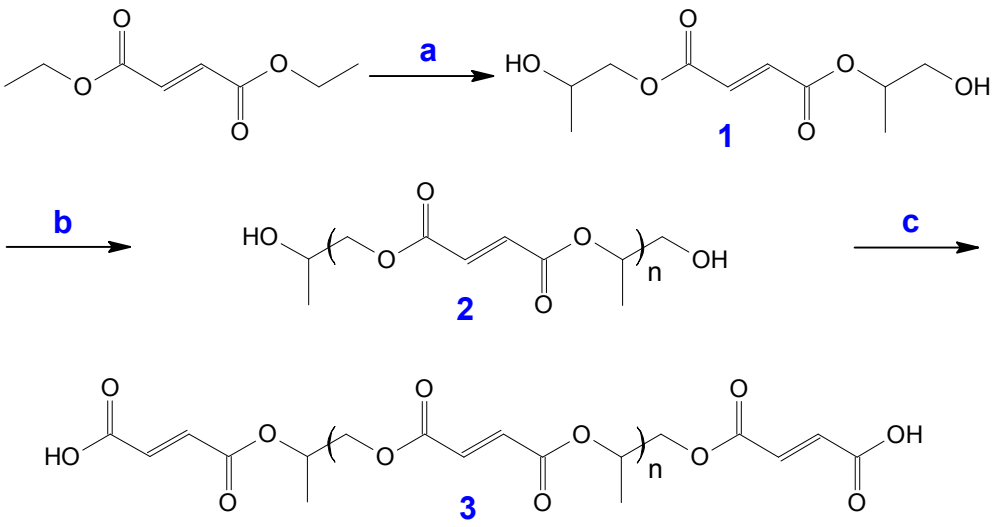

Scheme 2. Synthetic Scheme for the Preparation and Functionalization of PPF. Reagents and conditions: (a) propylene glycol, $ZnCl_2$, hydroquinone; (b) $ZnCl_2$, hydroquinone; (c) maleic anhydride, DMAP, DCM.

The synthesis and functionalization of PPF was confirmed by NMR (^1H, ^{13}C). The ^1H NMR spectra of propylene glycol and the synthesized PPF and MA-PPF are compared in Figure 1. There are four distinct peaks present in the spectrum of propylene glycol (Figure 1a), with the peaks at 1.16, 3.39 & 3.62, and 3.90 ppm attributed to the methyl (CH_3), methylene (CH_2), and methine (CH) protons, respectively. In the spectrum of PPF (Figure 1b), major peaks appeared at 6.85, 5.29, 4.33 & 4.25, and 1.34 ppm, attributable to the olefinic (O=C-C<u>H</u>=C<u>H</u>-C=O), methine, methylene, and methyl protons in the repeating unit, respectively. Some minor peaks are also present in the spectrum at 5.10, 4.22, 4.09, 3.70, 1.29, and 1.23 ppm, which are attributed to the end group of the PPF polymer chain (see Figure 1b). By integrating these major and minor peaks (Figure 2), the number average molecular weight ($\overline{M}_n$) of the synthesized PPF (**2**) was estimated as ~ 2200 Da, which is within the reported range between 500 and 4,000 Da.[31] When PPF was converted to MA-PPF (**3**), these major peaks were still present in the spectrum, but the minor peaks disappeared (Figure 1c). In addition, a minor broad peak appeared at 8.19 ppm in the ^1H NMR spectrum of MA-PPF, attributable to the carboxyl proton (-COO<u>H</u>) located at both ends of

the polymer chains. Together with the disappearance of the minor peaks present in the spectrum of PPF, this minor carboxyl peak in the ^{1}H NMR spectrum of MA-PPF suggested successful conversion of PPF to MA-PPF.

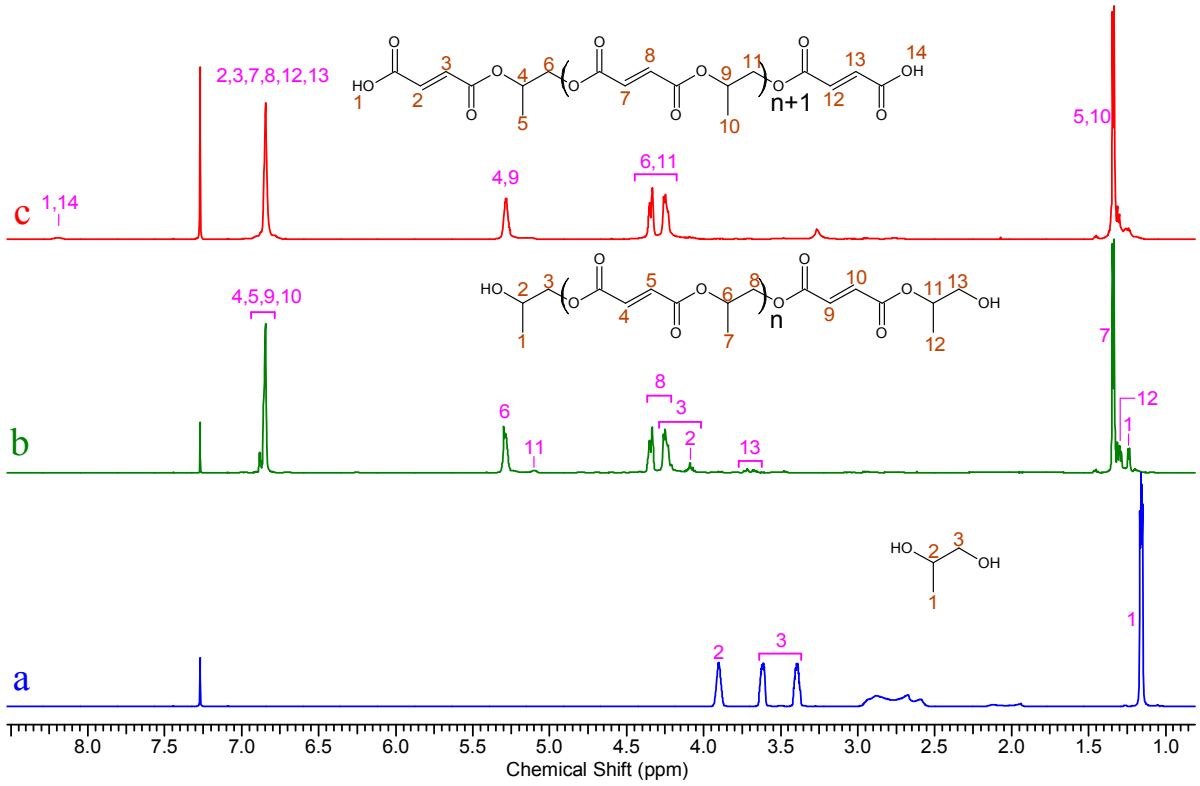

Figure 1. A comparison of ^{1}H NMR spectra of (a) propylene glycol, (b) the synthesized PPF, and (c) MA-PPF in $CDCl_3$.

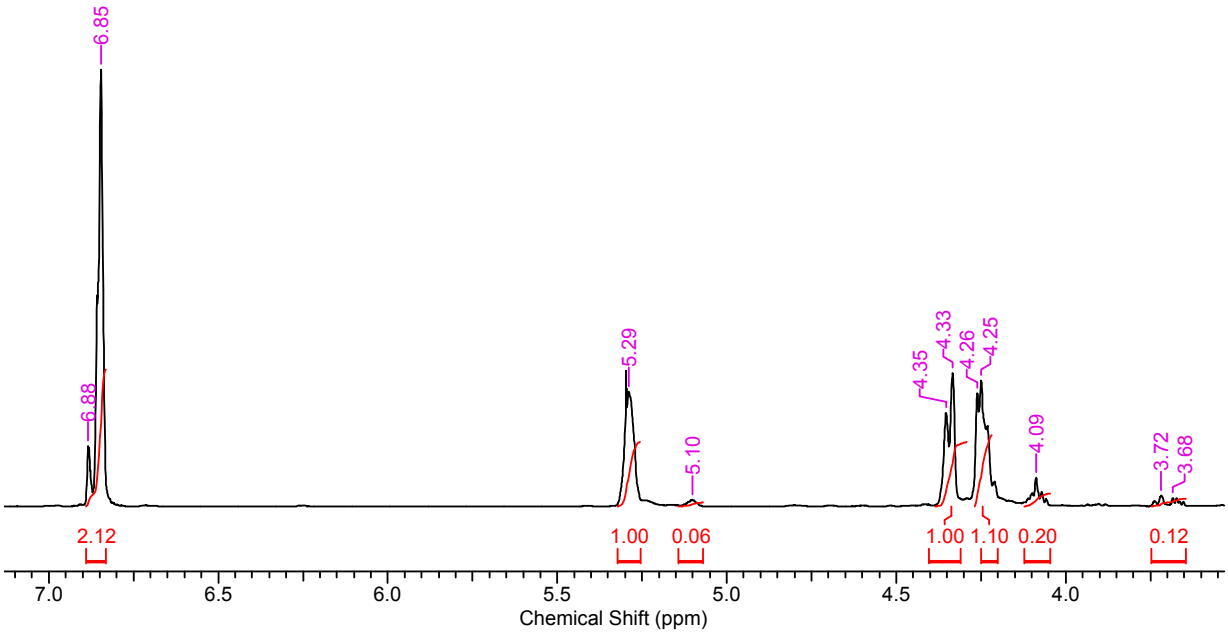

Figure 2. ^{1}H NMR spectrum of the synthesized PPF in $CDCl_3$ showing integrals of the peaks.

The successful conversion of PPF to MA-PPF was also evidenced by ^{13}C NMR results. A comparison of the ^{13}C spectra of propylene glycol, PPF, and MA-PPF is shown in Figure 3. In the spectrum of propylene glycol (Figure 3a), three carbon peaks appear at 68.2, 67.8, and 18.6 ppm, which are attributed to the methyl (CH_3), methylene (CH_2), and methine (CH) carbons, respectively. In the spectrum of PPF (Figure 3b), there are five major peaks appearing at 164.0-164.3, 133.3-134.0, 69.2, 66.6, and 16.3 ppm, attributable to the carbonyl (O=C-CH=CH-C=O), olefinic (O=C-CH=CH-C=O), methine, methylene, and methyl carbons in the repeating unit, respectively. Some minor peaks are also present in the spectrum at 73.1, 70.3, 65.8, 65.5, 19.2, and 16.0 ppm, which are attributed to the end group of the PPF polymer chains (Figure 3b). When PPF was converted to MA-PPF, these major peaks were still present but the minor peaks disappeared (Figure 3c). Although the peak of the carboxyl carbon at the end of the PPF-g-MA polymer chains was not observed due to its low concentration, the absence of the minor peaks in the spectrum of MA-PPF confirmed successful conversion of PPF to MA-PPF.

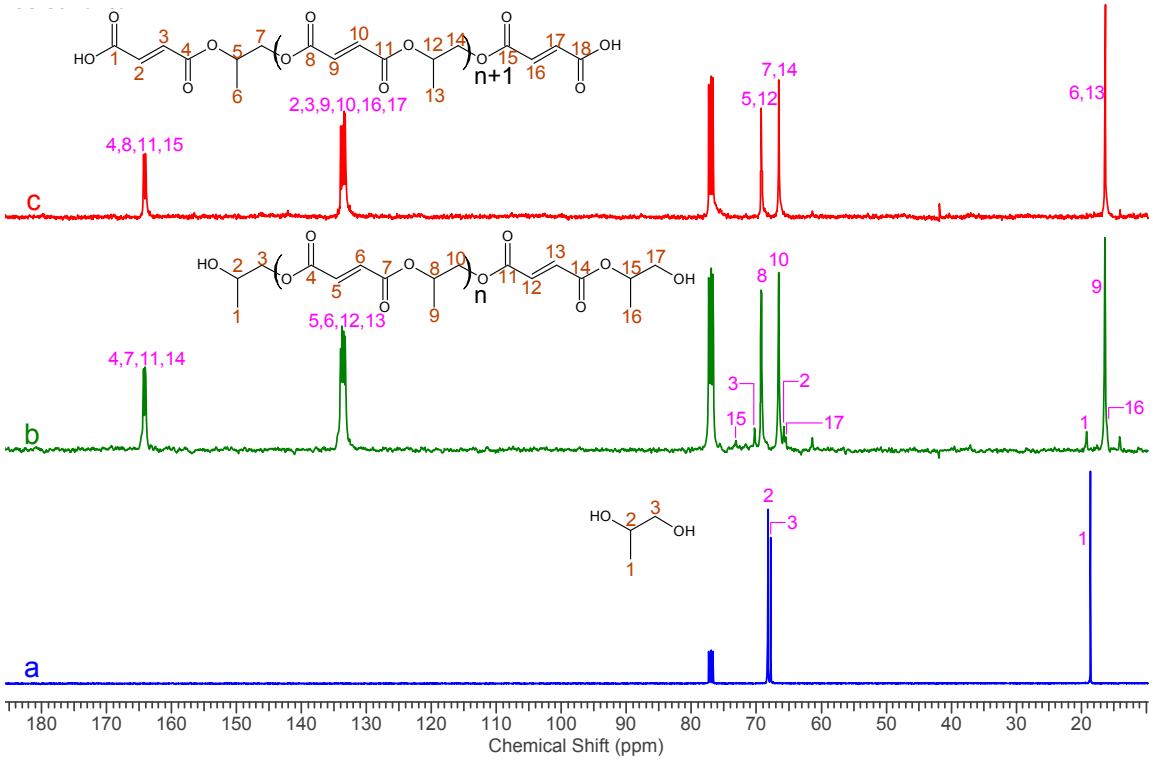

Figure 3. A comparison of ^{13}C NMR spectra of (a) propylene glycol, (b) the synthesized PPF, and (c) MA-PPF in $CDCl_3$.

3.2. Preparation of TiO_2-PPF nanocomposites and bone cement composites

To prepare TiO_2-PPF nanocomposites, TiO_2 nanowires/fibers were synthesized prior to reaction with **3**. The morphology and size of the nano-TiO_2 synthesized in $scCO_2$ and calcined at 450 °C were characterized by SEM and TEM, as shown in Figures 4a-b and Figure 4c-d, respectively. The mean diameter and aspect ratio of the synthesized fiber-like nanostructures of TiO_2 were determined to be 50 ± 10 nm and 30 ± 5, respectively (Figure 4c-d). These results are in good agreement with those reported in the literature.[32, 33] The advantage of this synthetic approach in $scCO_2$ is that high aspect ratio nanowires with high porosity and high surface area are produced.

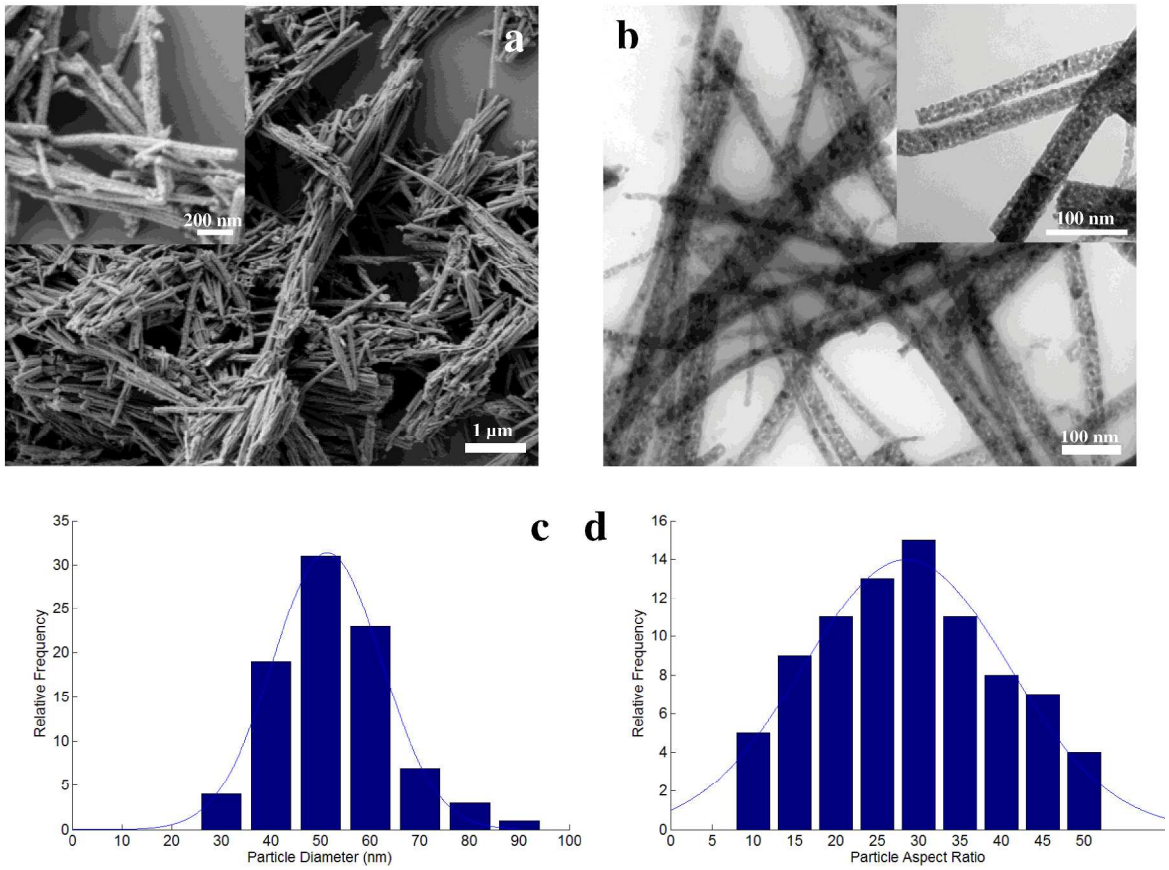

Figure 4. (a) SEM and (b) TEM images and the distribution of (c) diameter and (d) aspect ratio of the synthesized TiO_2 nanofibers.

With TiO_2 nanofibers being synthesized, TiO_2-PPF nanocomposites were prepared by coordination reaction of MA-PPF (**3**) to the surface of TiO_2 nanofibers, as shown in Scheme 3. The synthesized TiO_2-PPF nanocomposites (**4**) were further crosslinked to form the desired bone cement composites (**5**).

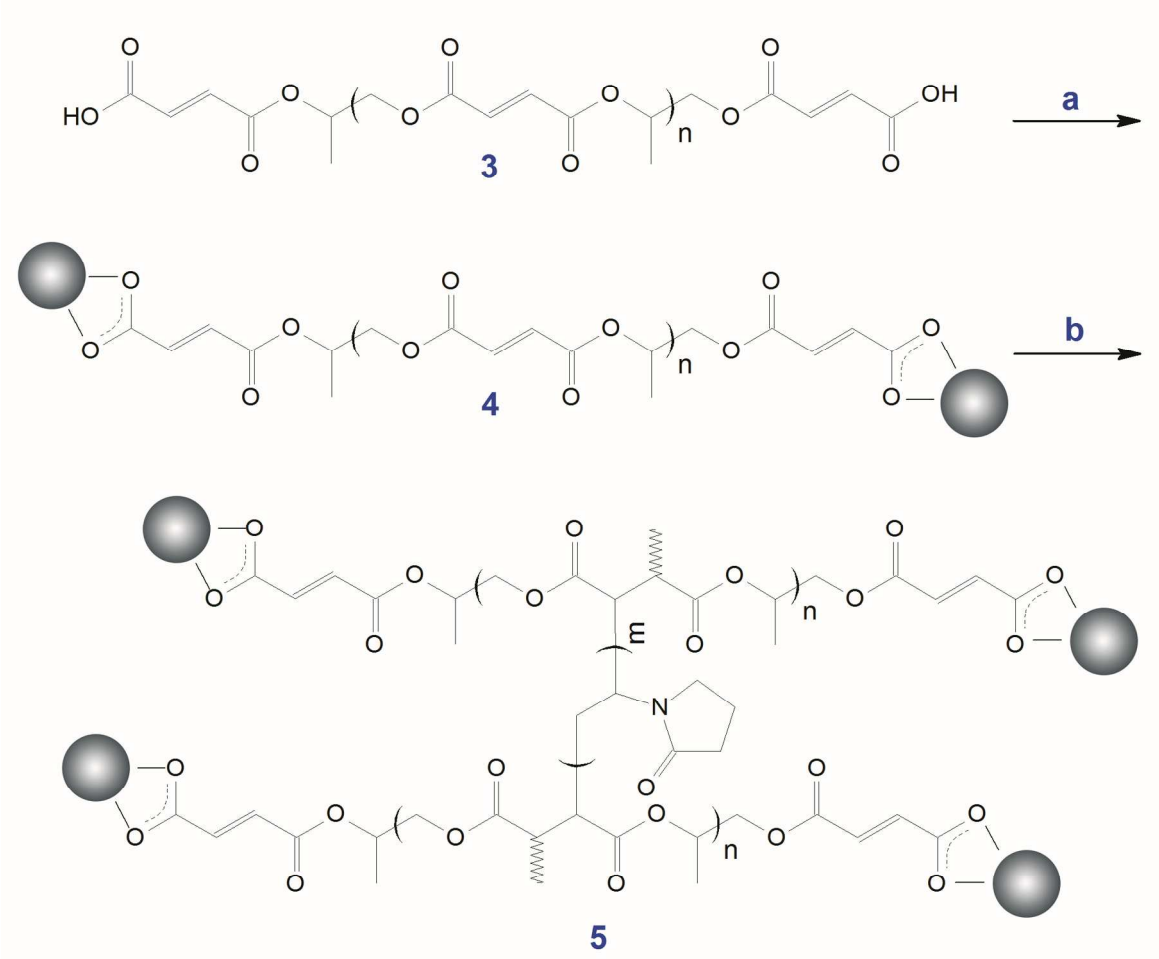

Scheme 3. Synthetic Scheme for the preparation of (4) TiO_2-PPF nanocomposites and (5) bone cement composites. Reagents and conditions: (a) TiO_2 nanofibers, THF; (b) N-VP, BPO, DMT.

The synthesized TiO_2-PPF nanocomposites (**4**) and cross-linked bone cement composites (**5**) were characterized with FTIR, XPS, and TGA to examine the reaction chemistry. The FTIR spectra of TiO_2, PPF, TiO_2-PPF nanocomposite (**4**), and bone cement composite (**5**) are compared in Figure 5. Several major characteristic peaks appeared at 1713, 1645, 1251, and 1148 cm^{-1} in the spectrum of PPF (Figure 5b), attributed to the C=O stretching, C=C stretching, asymmetric C-O-C stretching, and symmetric C-O-C stretching bands, respectively.[4, 34] The peak at 1645 cm^{-1} in the FTIR spectrum of both PPF and TiO_2-PPF nanocomposite shows the C=C

double bond was unaffected in the polymer chains after the reaction of MA-PPF and nano-TiO_2. Additional peaks appearing at 1570, 1377 and 1165 cm^{-1} in the FTIR spectrum of the TiO_2-PPF nanocomposite (Figure 5c) are attributed to the asymmetric and symmetric CO_2^- stretching bands, respectively, indicating successful coordination of PPF to the TiO_2 nanofibers. Rotzinger et al. described three possible coordination structures of carboxylate to the surface of TiO_2, i.e., chelating bidentate, monodentate, and bridging bidentate (Scheme 4).[34] These structures can be distinguished in infrared spectra by the separations between the carboxylate stretching bands ($\Delta\upsilon$). The band separation ($\Delta\upsilon$=405 cm^{-1}) between 1570 and 1165 cm^{-1} falls into the monodentate range (350-500 cm^{-1}) while another band separation ($\Delta\upsilon$=193 cm^{-1}) between 1570 and 1377 cm^{-1} might be indicative of a structure of bridging bidentate (150-180 cm^{-1}).[35] These coordination peaks remained evident in the spectrum of the crosslinked bone cement composite, although the peak at 1645 cm^{-1} (C=C stretching band) disappeared (Figure 5d). The disappearance of the C=C stretching band confirmed the crosslink reaction which consumed the C=C double bond (Scheme 3).[36]

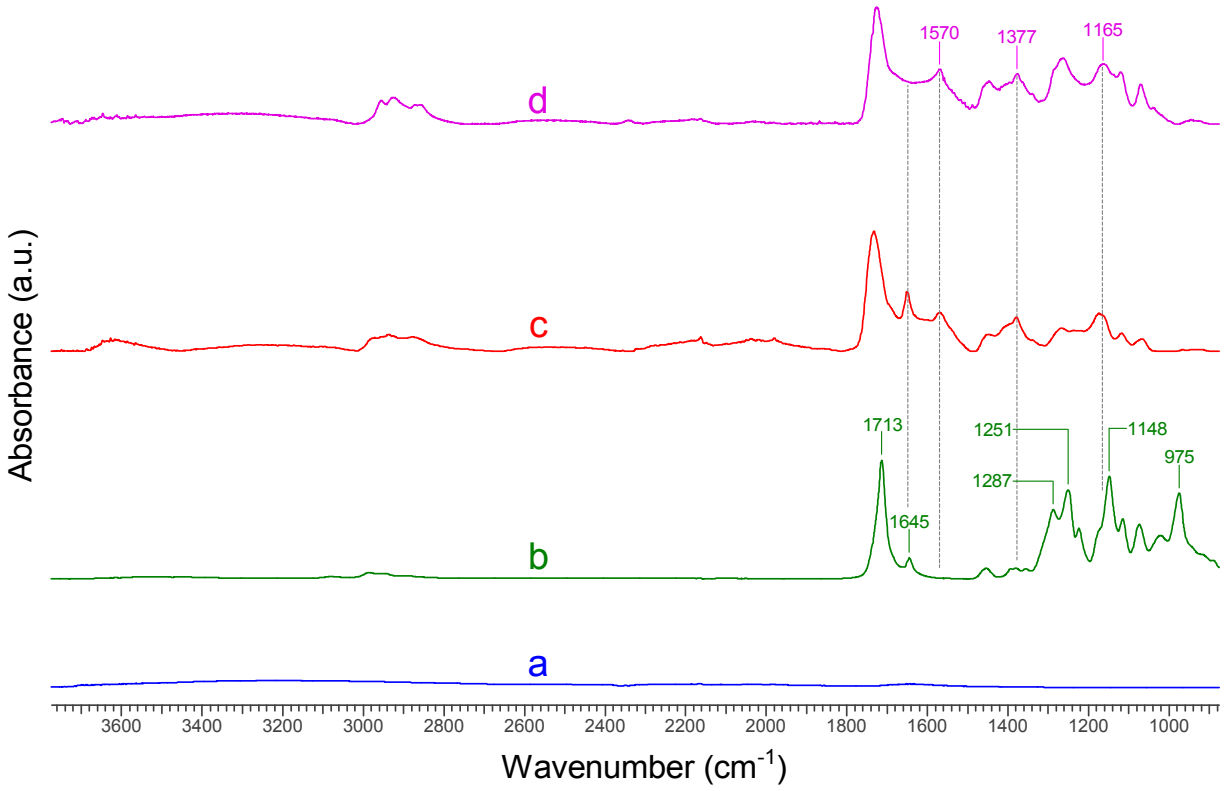

Figure 5. ATR-FTIR spectra of (a) TiO_2, (b) PPF, (c) TiO_2-PPF nanocomposite, and (d) crosslinked bone cement composite.

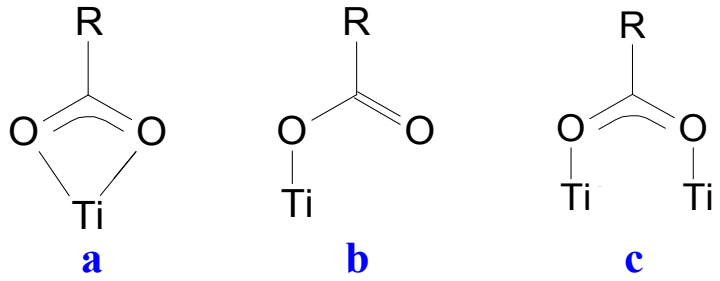

Scheme 4. Binding modes of RCOO- with TiO_2 surface (R= H or CH_3): (a) chelating bidentate (b) monodentate, and (c) bridging bidentate.[34]

X-ray photoelectron spectroscopy (XPS) was further employed for characterization of the synthesized PPF (**2**), MA-PPF (**3**), and non-crosslinked TiO_2-PPF (**4**) nanocomposites. The high resolution XPS scan of C 1s region for both PPF and MA-PPF (Figures 6a-b) represent similar patterns as expected for the chemistries involved. In both spectra, three major carbon peaks are

observed with binding energies of 285 eV, 286.5, and 289.0 eV, which correspond to aliphatic carbon (C–C, C-H), alcohol and ether functionality (C–OH, C–O–C), and ester and carboxylic acid type functionality (O–C=O), respectively [6] with relatively equal peak intensities for the peaks at 286.5 eV and 289.0 eV. Some of the intensity associated with the aliphatic carbon are attributed to adventitious carbon on the surface of the samples. In addition, the core level spectrum of O 1s for both PPF and MA-PPF, shown in Figures 6c-d, are resolved into two peaks at binding energies of 532 eV and 533.5 eV, which are attributed to O-C=O* and O*-C=O, respectively (* denotes the O of interest).[6]

In the recorded survey spectrum for the non-crosslinked TiO_2-PPF nanocomposite, the expected peaks for O, C, and Ti were detected (Figure 6e). In the high resolution XPS scan of the C 1s region (Figure 6f), the three major peaks observed for PPF and MA-PPF are still evident. In addition, a new peak appeared at 288.2 eV, which is assigned to the C atom of the carbonyl group from the successful covalent interaction of carboxylate to TiO_2.[37, 38] In order to verify the coordination of MA-PPF to the surface of TiO_2 nanofibers, a C 1s spectrum of the mechanically mixed TiO_2-PPF nanocomposite sample prepared by mechanical mixing of PPF (1g) with nano-TiO_2 (0.10 g) was measured (Figure 6g). As expected, no peak shifting or extra peaks were seen in the C 1s spectrum, indicating no chemisorption of PPF to the surface of nano-TiO_2. In the high resolution O 1s spectrum of non-crosslinked TiO_2-PPF-nanocomposite (Figure 6h), a new peak appeared at 529.3 eV, which is related to the lattice oxygen atoms in TiO_2 (Ti-O bonds).[39] Furthermore, the core level spectrum of Ti 2p for the non-crosslinked TiO_2-PPF-nanocomposite (Figure 7i) could be resolved into two spin-orbit pairs of 2p3/2 and 2p1/2 with binding energies of 458.3 eV and 464 eV, respectively, attributable to Ti^{4+} implying that the chemical state of

titanium remains as Ti^{4+}.[39, 40] Therefore, this XPS data confirms the successful coordination of MA-PPF to the surface of TiO_2 nanofibers without changing the state of nano-TiO_2.

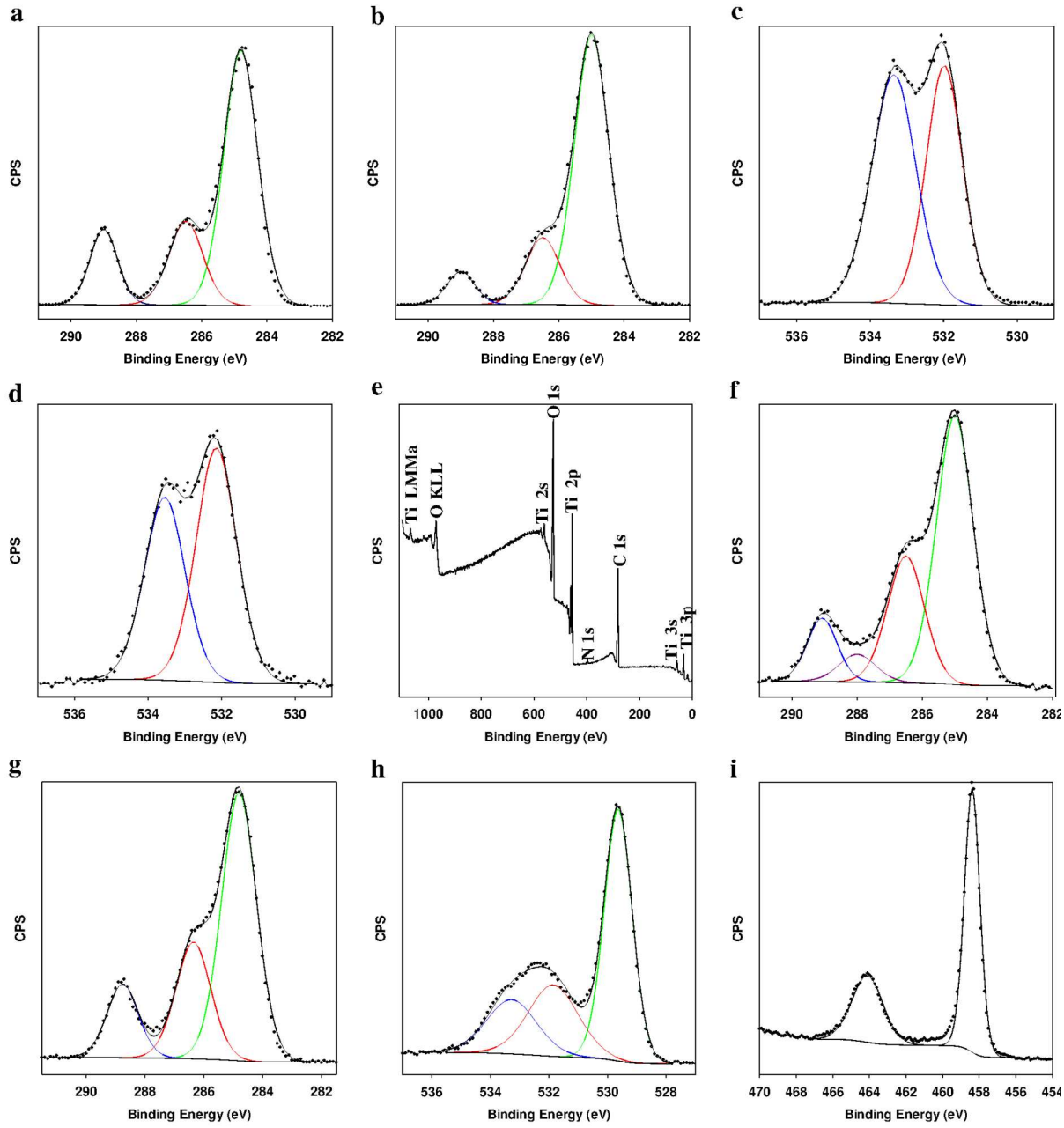

Figure 6. High resolution XPS record of C 1s region of (a) PPF and (b) MA-PPF, high resolution XPS record of O 1s region of (c) PPF and (d) MA-PPF, (e) XPS full-scan spectrum of the TiO_2-PPF nanocomposite, high resolution XPS scan of the C 1s region of (f) the TiO_2-PPF nanocomposite and (g) the mechanically mixed TiO_2-PPF nanocomposite, high resolution XPS scan of the O 1s region of (h) the TiO_2-PPF nanocomposite, and high resolution XPS scan of the Ti 2p region of (i) the TiO_2-PPF nanocomposite.

Thermogravimetric analysis (TGA) was also employed in the measurement of PPF attached to the surface of nano-TiO_2 in the synthesized TiO_2-PPF nanocomposites. The TGA characteristics of the nanocomposites are shown by the thermal weight loss and derivative of weight loss (DTG) of the composites with temperature. Figure 7 compares the calcined TiO_2, non-crosslinked PPF (**2**) and crosslinked PPF, non-crosslinked TiO_2-PPF (**4**) nanocomposites, and crosslinked TiO_2-PPF (**5**) bone cement composites. A typical TGA result of TiO_2-PPF nanocomposite shows two obvious regions when the temperature increased: the first region started from 30 °C and ended at 200 °C with a relatively small slope (due to evaporation of the entrapped water, solvent, or free carboxyl groups); while the second region started at 200 °C and ended at 400 °C with a large slope indicating more weight loss, which is attributed to the random internal scission of the PPF chains chemically attached to the TiO_2 nanoparticles. The sample of TiO_2-PPF nanocomposite displayed a weight loss of 74% compared to the calcined TiO_2 with the weight loss of 3%. PPF functionalization allowed a relatively high number of polymer chains to be attached on the surface of TiO_2 nanofibers, resulting in an increased weight loss for the TiO_2-PPF nanocomposites.

In addition, the effect of functionalization of the PPF on the nanocomposites can be observed by an enhanced thermal stability of the synthesized bone cement composite compared to the unmodified PPF. As shown in Figure 8, the onset degradation temperature T_d for non-crosslinked PPF, crosslinked PPF, TiO_2-PPF nanocomposites, and bone cement composite is 332 ºC, 345 ºC, 336 ºC, and 355 ºC, respectively, with bone cement composite representing the highest thermal dissociation temperature. This thermal stability enhancement is attributed to the strong interfacial adhesion between the nano-TiO_2 and PPF matrix, which results from the excellent chemical interaction of nano-TiO_2 and functionalized polymer chains, with this strong

adhesion providing a barrier effect to the polymer molecules evaporated during the thermal degradation of the nanocomposites.

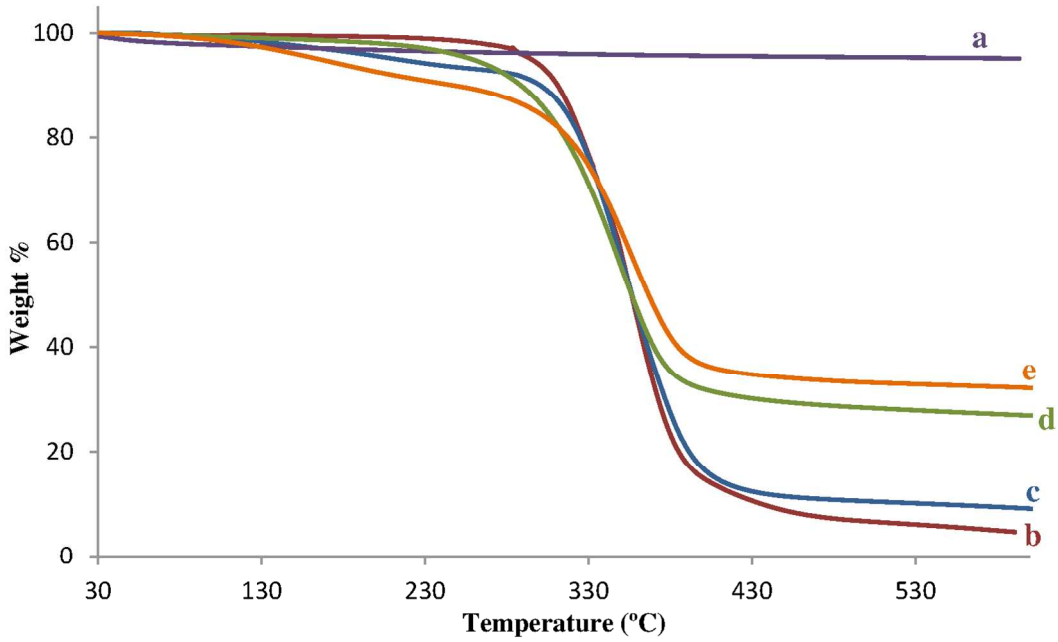

Figure 7. TGA curves of: (a) TiO_2, (b) PPF, (c) crosslinked PPF, (d) TiO_2-PPF nanocomposite (synthesized using 1 g of MA-PPF and 0.0250 g of TiO_2) and (e) crosslinked bone cement composite (made of 1 g of TiO_2-PPF synthesized using 0.0250 g of TiO_2).

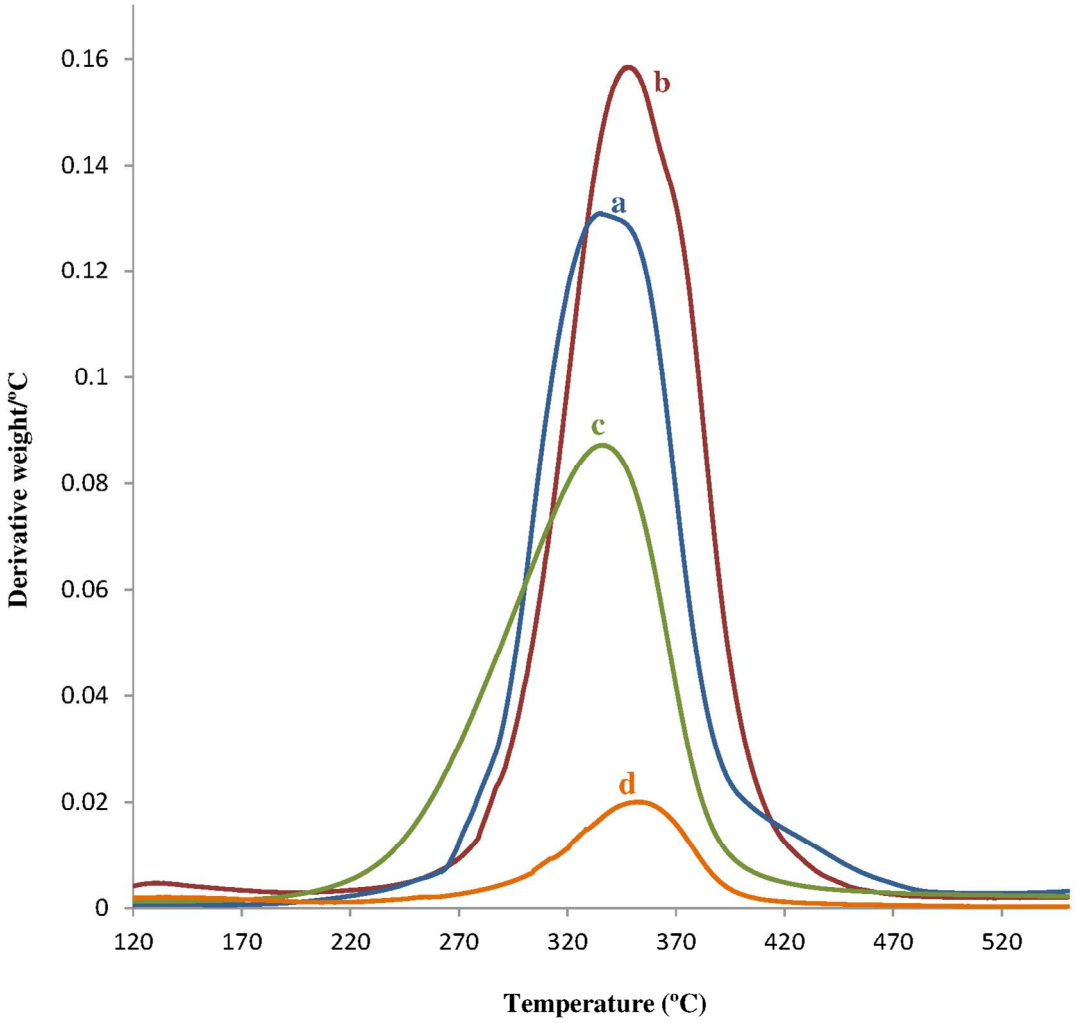

Figure 8. Derivative thermogravimetric (DTG) curves of: (a) PPF, (b) crosslinked PPF, (c) (d) TiO_2-PPF nanocomposite (synthesized using 1 g of MA-PPF and 0.0250 g of TiO_2) and (e) crosslinked bone cement composite (made of 1 g of TiO_2-PPF synthesized using 0.0250 g of TiO_2).

3.3. Mechanical properties of crosslinked PPF and bone cement composites

The Young's modulus and tensile strength were measured for the crosslinked PPF and bone cement composites with varying nanowire-TiO_2 concentrations, and mechanically mixed bone cement composites. The incorporation of nano-TiO_2 reinforced the mechanical properties of the PPF, as shown in Table 3. The Young's modulus and ultimate tensile strength of crosslinked composites increased with the initial relatively low concentrations of TiO_2, peaked

for bone cement composite-1 and bone cement composite-2, and then plateaued or decreased at higher loading concentrations. There was a 2.5-fold increase in the Young's modulus for the bone cement composite-1 compared to the pure polymer. Moreover, the tensile strength, similar to the Young's modulus, decreased with loading of nano-TiO_2 over 0.5-1% in the starting composition. It is clear from Table 3 that bone cement composite-1 (Sample 2) possesses the highest value of Young's modulus and ultimate tensile strength amongst the different composites tested. This high value of Young's modulus and tensile strength is attributed to the strong interfacial bonding of the functionalized PPF with nano-TiO_2 fibers as shown by Figure 9, which facilitates the transfer of interfacial stress from the filler to the matrix. It can be seen that the unfilled polymer exhibited a smooth plain surface (Figure 9a). while the bone cement composite-1 showed a rough surface with the nano-TiO_2 fibers delaminated from the PPF matrix (Figure 9b). Figure 9b also reveals that the individual nano-TiO_2 fibers were dispersed homogeneously throughout the bone cement composite-1, with strong adhesion to the matrix when reacted to the PPF after being functionalized. The dispersion of individual nanofibers in a polymer matrix may prevent slippage between TiO_2 nanowires while enhancing the transfer of applied load to the nano-TiO_2, which further enhances the mechanical reinforcement. This synthesis methodology provided better compatibility with nano-TiO_2 while establishing chemical bonding through the carboxylic group, resulting in strong interfacial adhesion between the fibers and the matrix as the partially broken or pulled out fibers on their surface is shown by the arrows in Figure 9b. In addition to the strong adhesion with the matrix, these partially pulled out fibers are also shown to bridge the cracks in the matrix (Figure 9c). However, at higher loading concentration (bone cement composite-2**)**, the measured mechanical properties of these nanocomposites began to decline. This is attributed to the nano-TiO_2 fibers agglomerating at higher concentrations within

the polymer matrix, i.e., 10 wt% (Figure 9d). The formed agglomerates are considered to be responsible for accelerating crack propagation through local stress concentrators (voids).

Table 3. Mechanical Properties of the crosslinked PPF and the synthesized bone cement composites.

*Sample	**TiO_2 (g) for 1 g of MA-PPF	***TiO_2 (g) for 1 g of PPF	Young's modulus (MPa)	Offset yield 1% (MPa)	Tensile strength (MPa)	Flexural modulus (MPa)	Flexural strength (MPa)
1	0		228 ± 42	6.2 ± 2.3	10.6 ± 2.1	365 ± 66	18.8 ± 2.6
2	0.005		578 ± 37	17.3 ± 0.9	22.6 ± 2.9	1084 ± 115	42.5 ± 6.1
3	0.0125		512 ± 26	15.5 ± 3.6	22.3 ± 3.3	815 ± 83	35.9 ± 0.5
4	0.0250		378 ± 65	14.5 ± 0.6	15.8 ± 0.9	983 ± 34	28.2 ± 6.8
5		0.05	318 ± 40	6.8 ± 2.5	14.7 ± 1.4	583 ± 58	20.6 ± 8.7

Note: the average values and deviations were calculated from 5 sets of repeating experiments.
* The sample number corresponds to the entry number in Table 2. ** The TiO_2 concentration corresponds to the amount of nanowires/fibers used for the formation of TiO_2-PPF nanocomposites, presented in detail in Table 1. *** The TiO_2 concentration corresponds to the actual TiO_2 concentration in the TiO_2-PPF nanocomposite-1 obtained by TGA analysis represented in Table 1.

In addition, flexural modulus and flexural strength values of the bone cement composite reflect its resistance to flexural loading which is a combination of tension and compression forces. Similarly, dramatic reinforcements in the flexural properties (FS and FM) were achieved with bone cement composites, as evident in Table 3. This extraordinary mechanical reinforcement provided by bone cement composites exceeded the enhancements observed with

the mechanically mixed bone cement composite (Sample 5), indicating the importance of mechanical coupling between the nanowire and the functionalized PPF matrix. Bone cement composite-1 formulation exhibited a roughly 3-fold increase in flexural modulus and a greater than 2-fold increase in flexural strength compared to blank polymer. Loadings beyond 0.5 wt% nano-TiO_2 in the starting material led to a decrease in the flexural properties of these bone cement composites, due in part to aggregation of nanowires (Figure 9d).

Due to the complexity of bone cement preparation chemistry including the type of polymers, nanofillers, and crosslinking agents, as well as the loading concentration, it is difficult to compare their mechanical properties. Previously Khaled et al. prepared bone cement materials by incorporating TiO_2-SrO nanotubes into PMMA, achieving a flexural modulus of 2220 ± 100 MPa and a flexural strength 69.98 ± 1.40 MPa.[41] The highest flexural modulus and flexural strength measured in the present study are 1084 ± 115 MPa and 42.5 ± 6.1 MPa, respectively. These values are comparable with those obtained by utilizing high molecular weight PMMA (207 kDa),[41] although much lower molecular weight of PPF (2.2 kDa) was employed in this study. Studies employing functionalized single-walled carbon nanotubes in PPF matrix showed a flexural modulus of 769 ± 114 MPa and a flexural strength of 42.8 ± 3.7 MPa,[16] although the crosslinker used in their work, poly(propylene fumarate)-diacrylate (PPF-DA), may also be contributing to the reported improved mechanical properties. Considering previously reported flexural modulus of human trabecular bone, our results show that TiO_2-PPF nanocomposites have sufficient mechanical strength for bone tissue engineering applications.[17]

It should be noted that nano-titania is an established biocompatible material.[28, 41] The maleic anhydride-functionalized PPF having two small functional groups at each end of a biocompatible polymer (PPF) chain should also be biocompatible. Hence, the prepared TiO_2-PPF

bone cement materials are expected to be biocompatible; however, a future study will be needed to further explore the biocompatibility of functionalized-PPF and TiO_2-PPF bone cement composites. From the above discussion it can be deduced that TiO_2 nanofibers can act as an excellent reinforcing agent for an experimental functionalized PPF matrix in order to produce a new generation of bone cements. Chemical bonding between the filler and the polymer helps the resulting bone cement composites exhibit significantly enhanced mechanical properties. In addition, a study of degradation behavior of the prepared bone cement composites is planned as the next stage for this work.

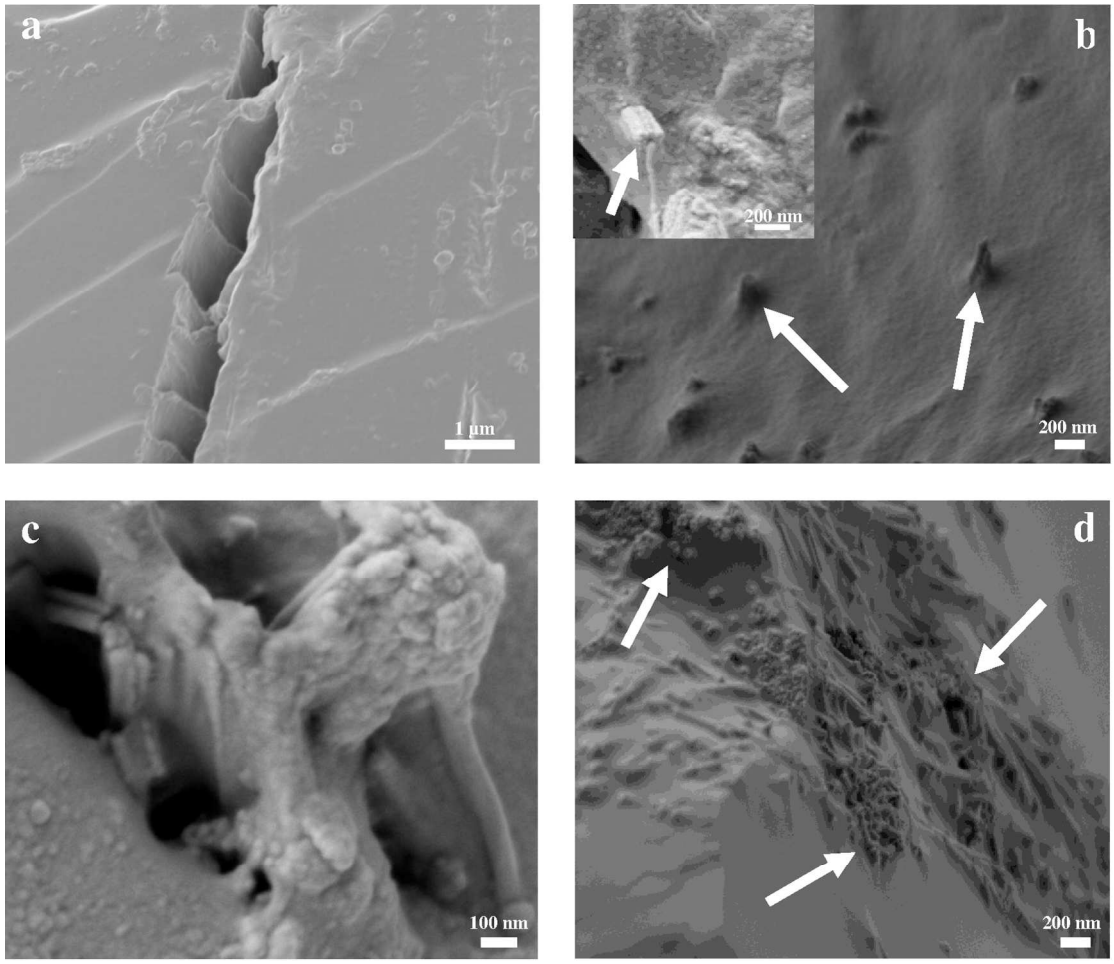

Figure 9. SEM images of the fracture planes of (a) crosslinked unmodified PPF, (b) bone cement composite-1, (c) crack bridging within the bone cement composite-1, and (d) bone cement

composite-2, (the arrows show TiO_2 nanofibers are covered by polymer and aligned perpendicularly to the fracture surface).

CONCLUSION

Biodegradable poly(propylene fumarate) (PPF) was synthesized and then functionalized with maleic anhydride. Successful synthesis and functionalization of PPF was confirmed by ^{1}H and ^{13}C NMR and XPS. The functionalized PPF was grafted to the surface of TiO_2 nano-fibers synthesized using a sol-gel reaction in supercritical CO_2. Bone cement composites were obtained by polymerization of the PPF-grafted nano-TiO_2 and a crosslinker N-vinylpyrrolidone. The polymerization was confirmed by FTIR while TGA results revealed improved thermal stability of the crosslinked bone cement composites. Mechanical testing demonstrated much enhanced tensile and flexural properties of the bone cement composites after the incorporation of TiO_2 nano-fiber into the polymer matrix, suggesting potential application in bone cementation.

ACKNOWLEDGMENT

The authors would like to thank Dr. Todd Simpson of the Nanofabrication Laboratory at the University of Western Ontario (UWO) for SEM analysis, Dr. Richard Gardiner of Biotron at UWO for the TEM work, and Mr. Yixing Tang of the Department of Chemical and Biochemical Engineering department at UWO for sharing his knowledge of TGA analysis. Graphical abstract was prepared with the help of Dr. Serge Ayissi of the Department of Chemical and Biochemical Engineering at UWO. Financial funding was provided from OGIRC and the Canadian Foundation for Innovation (CFI).

References

1. N. J. Shah, Hyder, M.N., Moskowitz, J.S., Quadir,M.A., Morton, S.W., Seeherman,H. J., Padera,R. F., Spector,M., Hammond, P.T., *Sci Transl Med*, 2013, 5, 1-10.
2. G. Kaur, O. P. Pandey, K. Singh, D. Homa, B. Scott and G. Pickrell, *Journal of Biomedical Materials Research Part A*, 2014, 102, 254-274.
3. M. L. Wood, C. M. McDowell and S. S. Kelley, *Clinical orthopaedics and related research*, 2003, 412, 94-102.
4. C.-H. Chang, T.-C. Liao, Y.-M. Hsu, H.-W. Fang, C.-C. Chen and F.-H. Lin, *Biomaterials*, 2010, 31, 4048-4055.
5. K. Goto, J. Tamura, S. Shinzato, S. Fujibayashi, M. Hashimoto, M. Kawashita, T. Kokubo and T. Nakamura, *Biomaterials*, 2005, 26, 6496-6505.
6. P. Maiti, G. Kapusetti, N. Misra, V. Singh, S. Srivastava, P. Roy and K. Dana, *Journal of Materials Chemistry B*, 2014.
7. C. Fang, R. Hou, K. Zhou, F. Hua, Y. Cong, J. Zhang, J. Fu and Y.-J. Cheng, *Journal of Materials Chemistry B*, 2014.
8. G. Lewis, *J. Biomed. Mater. Res. B Appl. Biomater.* , 2007, 84, 301–319.
9. N. Anitha, V. Thomas and M. Jayabalan, *Journal of the Indian Institute of Science*, 2013, 79, 431.
10. A. M. Henslee, D. H. Gwak, A. G. Mikos and F. K. Kasper, *Journal of Biomedical Materials Research Part A*, 2012, 100, 2252-2259.
11. D. L. Alge, J. Bennett, T. Treasure, S. Voytik‐Harbin, W. S. Goebel and T. M. G. Chu, *Journal of Biomedical Materials Research Part A*, 2012, 100, 1792-1802.
12. S. He, M. Timmer, M. Yaszemski, A. Yasko, P. Engel and A. Mikos, *Polymer*, 2001, 42, 1251-1260.
13. W. Zhao, D. Yang, Z. Li and T. Xu, *Sheng wu yi xue gong cheng xue za zhi= Journal of biomedical engineering= Shengwu yixue gongchengxue zazhi*, 2005, 22, 381.
14. A. K. Shung, M. D. Timmer, S. Jo, P. S. Engel and A. G. Mikos, *Journal of Biomaterials Science, Polymer Edition*, 2002, 13, 95-108.
15. J. P. Fisher, T. A. Holland, D. Dean and A. G. Mikos, *Biomacromolecules*, 2003, 4, 1335-1342.
16. X. Shi, J. L. Hudson, P. P. Spicer, J. M. Tour, R. Krishnamoorti and A. G. Mikos, *Nanotechnology*, 2005, 16, S531.
17. R. A. Horch, N. Shahid, A. S. Mistry, M. D. Timmer, A. G. Mikos and A. R. Barron, *Biomacromolecules*, 2004, 5, 1990-1998.
18. D. Hakimimehr, D.-M. Liu and T. Troczynski, *Biomaterials*, 2005, 26, 7297-7303.
19. K.-W. Lee, S. Wang, M. J. Yaszemski and L. Lu, *Biomaterials*, 2008, 29, 2839-2848.
20. C. C. Wu, K. C. Yang, S. H. Yang, M. H. Lin, T. F. Kuo and F. H. Lin, *Artificial organs*, 2012, 36, 418-428.
21. B. Sitharaman, X. Shi, X. F. Walboomers, H. Liao, V. Cuijpers, L. J. Wilson, A. G. Mikos and J. A. Jansen, *Bone*, 2008, 43, 362-370.
22. S. Khaled, R. Sui, P. A. Charpentier and A. S. Rizkalla, *Langmuir*, 2007, 23, 3988-3995.
23. S. Khaled, P. A. Charpentier and A. S. Rizkalla, *Journal of Biomaterials Applications*, 2011, 25, 515-537.
24. A. Mistry, A. Mikos and J. Jansen, *Journal of Biomedical Materials Research Part A*, 2007, 83, 940-953.
25. P. Li, C. Ohtsuki, T. Kokubo, K. Nakanishi, N. Soga and K. de Groot, *Journal of biomedical materials research*, 1994, 28, 7-15.
26. N. Trabandt, G. Brandes, E. Wintermantel, T. Lenarz and M. Stieve, *Otology & Neurotology*, 2004, 25, 682-693.

27. M. Uchida, H. M. Kim, T. Kokubo, S. Fujibayashi and T. Nakamura, *Journal of Biomedical Materials Research Part A*, 2003, 64, 164-170.
28. S. Khaled, R. J. Miron, D. W. Hamilton, P. A. Charpentier and A. S. Rizkalla, *dental materials*, 2010, 26, 169-178.
29. J. West, A. Brennan, A. Clark, M. Zamora and L. Hench, *Journal of biomedical materials research*, 1998, 41, 8-17.
30. A. C. Spivey and B. I. Andrews, *Angewandte Chemie International Edition*, 2001, 40, 3131-3134.
31. F. K. Kasper, K. Tanahashi, J. P. Fisher and A. G. Mikos, *Nature protocols*, 2009, 4, 518-525.
32. R. Sui, A. S. Rizkalla and P. A. Charpentier, *Langmuir*, 2005, 21, 6150-6153.
33. R. Sui, A. S. Rizkalla and P. A. Charpentier, *The Journal of Physical Chemistry B*, 2006, 110, 16212-16218.
34. F. P. Rotzinger, J. M. Kesselman-Truttmann, S. J. Hug, V. Shklover and M. Grätzel, *The Journal of Physical Chemistry B*, 2004, 108, 5004-5017.
35. K. D. Dobson and A. J. McQuillan, *Spectrochimica Acta Part A: Molecular and Biomolecular Spectroscopy*, 1999, 55, 1395-1405.
36. M. Jayabalan, *International journal of biomaterials*, 2009, 2009.
37. X. Wu, D. Wang and S. Yang, *Journal of colloid and interface science*, 2000, 222, 37-40.
38. B. Hojjati and P. A. Charpentier, *Journal of Polymer Science Part A: Polymer Chemistry*, 2008, 46, 3926-3937.
39. M. C. Biesinger, L. W. Lau, A. R. Gerson and R. S. C. Smart, *Applied Surface Science*, 2010, 257, 887-898.
40. N. Farhangi, R. R. Chowdhury, Y. Medina-Gonzalez, M. B. Ray and P. A. Charpentier, *Applied Catalysis B: Environmental*, 2011, 110, 25-32.
41. S. Khaled, P. A. Charpentier and A. S. Rizkalla, *Acta biomaterialia*, 2010, 6, 3178-3186.

Table of Content only

Synthesis and characterization of novel TiO_2-poly(propylene fumarate) nanocomposites for bone cementation

Mehrnaz Salarian[1], William Z. Xu[2], Mark C. Biesinger[3], and Paul A. Charpentier[1, 2, *]

A novel composite material made from poly(propylene fumarate) (PPF) and titania nanofibers has been synthesized for potential use as an orthopaedic biomaterial with TiO_2 nanofibers chemically linked to the PPF matrix as a reinforcing phase to enhance its mechanical properties.